Comparison of the Influence of Different Compatibilizers on the Structure and Properties of Ethylene Vinyl Acetate Copolymer/Modified Clay Nanocomposites

B. R. Guduri,[1,2] A. S. Luyt[1]

[1]*Department of Chemistry, University of the Free State, Qwaqwa Campus, Private Bag X13, Phuthaditjhaba, 9866, South Africa*
[2]*Materials Science and Manufacturing, Polymers, Ceramics, and Composites Division, Council for Scientific and Industrial Research, P.O. Box 395, Pretoria 0001, South Africa*

Received 14 October 2006; accepted 27 March 2007
DOI 10.1002/app.26532
Published online 5 June 2007 in Wiley InterScience (www.interscience.wiley.com).

ABSTRACT: Nanocomposites of an ethylene vinyl acetate copolymer and clay were prepared by melt blending and extrusion. Two different compatibilizers, ethylene glycidyl methacrylate (EGMA) and maleic anhydride grafted polypropylene (MAPP), were used in these nanocomposites. The structural properties of the composites were characterized with X-ray diffraction and transmission electron microscopy. The surface morphology was characterized with polarized optical microscopy. The tensile and permeability properties were studied. The thermal stability of the nanocomposites was characterized through thermogravimetric analysis. MAPP-compatibilized nanocomposites had intercalated and partially exfoliated structures, whereas EGMA-compatibilized nanocomposites had completely exfoliated structures. The EGMA-compatibilized nanocomposites were thermally more stable than the MAPP-compatibilized nanocomposites. The mechanical and permeability properties of the EGMA-compatibilized nanocomposites were better than those of the MAPP-compatibilized nanocomposites. © 2007 Wiley Periodicals, Inc. J Appl Polym Sci 105: 3612–3617, 2007

Key words: gas permeation; mechanical properties; nanolayers; organoclay; thermogravimetric analysis (TGA)

INTRODUCTION

Nanocomposites have attracted much attention in recent years because their electrical, mechanical, optical, and other physicochemical properties can often be modified favorably on account of nanometer-level interphase interactions and quantum effects.[1,2] Much work has therefore been focused on developing polymer–clay nanocomposites with various polymers.[3–12] Depending on the clay type and chemical structure of the polymer, several methods have been developed to synthesize polymer–clay composites. The first polymer–clay nanocomposite was successfully synthesized with a polymer containing polar groups, which allowed the clay to disperse readily.[13] Nanocomposites have at least one ultrafine phase dimension typically in the range of 1–100 nm and exhibit improved properties in comparison with microcomposites and macrocomposites. Strong interfacial interactions between the dispersed clay layers and the polymer matrix lead to enhanced mechanical, thermal, and barrier properties of the virgin polymer.[14,15]

The clay in a nanocomposite may be intercalated or exfoliated or have a mixed morphology, depending on the degree of dispersion of the clay layers.[16,17] Various polymer systems have been used to form nanocomposites of a polymer and montmorillonite (MMT).[18,19] Alexandre et al.[18] prepared ethylene vinyl acetate copolymer (EVA) based nanocomposites by melt intercalation and also showed that sodium MMT and MMT modified with ammonium cations bearing a carboxylic acid moiety were not suitable for EVA nanocomposites. Zanetti et al.[19] reported the collapse of the interlayer of octadecylammonium-modified MMT in an EVA matrix. Zhang and Wilkie[20] synthesized a polyethylene–clay nanocomposites by melt intercalation, using maleic anhydride grafted polyethylene as a compatibilizer. Their results indicated that the clay in the composite was barely intercalated.[21,22] Lee et al.[23] prepared polyethylene–clay nanocomposites with maleic anhydride grafted polypropylene (MAPP) as a compatibilizer, and they observed better exfoliation and mechanical properties of the nanocomposites.

Correspondence to: A. S. Luyt (luytas@qwa.uovs.ac.za).
Contract grant sponsor: South African National Research Foundation; contract grant number: GUN 2070099.
Contract grant sponsor: University of the Free State.

Journal of Applied Polymer Science, Vol. 105, 3612–3617 (2007)

The aim of this work was to compare the effects of an ethylene glycidyl methacrylate (EGMA) copolymer and MAPP compatibilization on the physical properties of EVA–clay nanocomposites. The nanocomposites were prepared by melt blending and extrusion. The morphology of the nanocomposites was characterized with X-ray diffraction (XRD) and transmission electron microscopy (TEM). The mechanical, gas permeability, thermal stability, and surface properties of the nanocomposites were compared.

EXPERIMENTAL

Materials

EVA with 9% vinyl acetate was supplied by Plastamid (Elsies River, South Africa). According to the supplier, it had a melting point of 95°C, a density of 0.930 g/cm^3, a tensile strength of 19.0 MPa, and an elongation at break of 750%.

EGMA was supplied by Plastamid. According to the supplier, it had a melting point of 93°C, a density of 0.94 g/cm^3, a tensile strength of 12 MPa, and an elongation at break of 440%. MAPP (MAPP-OPTIM-415; maleic anhydride reactive modifier content = 1 wt %) was supplied by Pluss Polymers (Delhi, India).

Cloisite 15A clay (ditallow dimethyl ammonium salts of bentonite), supplied by Southern Clay Products (Gonzales, TX), was used as a reinforcement. The as-received clay particles were disklike stacks of thin silicate layers, 1 nm thick and ranging in diameter from 100 nm to several micrometers. The specific gravity of the clay particles (stacks) was 1.6–1.8 g/cm^3.

Preparation of the nanocomposites

The EVA and compatibilizer were mixed at 160°C and 60 rpm for 10 min in a Brabender 55-mL mixing chamber (Duisburg, Germany) to obtain a well-mixed blend, after which the clay was added. The total mixing time was 20 min. This was followed by extrusion into films 0.45 ± 0.05 mm thick in a Brabender single-screw extruder (extruder screw speed = 30 rpm).

Characterization of the samples

The degree of intercalation or exfoliation was evaluated with XRD. XRD patterns of the nanocomposite samples were obtained with a Bruker-AXS (Madison, WI) D8 Advance X-ray diffractometer with Cu Kα radiation (wavelength = 1.5406 Å). The detector was an Na–I scintillation counter with a monochromator.

The TEM analyses were conducted on a JEOL JEM-100CX II electron microscope (Tokyo, Japan). A Sorvall MT6000 microtome was used to cut thin sections (<100 nm thick) of the samples at room temperature.

Oxygen permeability measurements were carried out on 80 × 40 × 2 mm^3 samples in a setup connected to a Smart-Trek series 100 digital mass flow meter (Sierra Instruments, Inc., Monterey, CA), which guaranteed high measurement accuracy (±0.7%).

A Hounsfield H5KS universal testing machine (Redhill, England) was used to investigate the tensile properties of the nanocomposites. Samples of 150 mm × 15 mm × 0.45 mm were analyzed at a crosshead speed of 10 mm/min. A continuous load–deflection curve was obtained. In each case, 10 samples were used, and the average was taken.

Thermogravimetric analysis (TGA) was performed on a PerkinElmer TGA 7 thermogravimetric analyzer (Wellesley, MA). The experiments were carried out from 30 to 600°C at a heating rate of 10°C/min. The experiments were performed under a nitrogen atmosphere at a flow rate of 20 mL/min.

The polarized optical microscopy photographs of the nanocomposites were recorded with a CETI light microscope supplied by Scientific Instruments, Ltd. (England). A digital camera (DCM35), supplied by Laboratory and Scientific Equipment (Pty.), Ltd. (Durban, South Africa), was used for the photographs.

RESULTS AND DISCUSSION

For EVA–Cloisite 15A clay nanocomposites, we found in a previous study[24] that the clay was intercalated in samples containing 2–5% clay (Table I) but that a sample containing 1% clay showed a mixed intercalated and exfoliated structure with a somewhat larger basal spacing. For these samples, the tensile strength and elongation slightly decreased, whereas the tensile modulus substantially increased with increasing clay content.

Generally, when maleic anhydride grafted compatibilizers are used, the maleic anhydride group interacts with the swelling agent in organically modified MMT and helps the polymer molecules penetrate the clay interlayer more easily.[23] Figure 1(C,D) shows the XRD spectra of 10% MAPP compatibilized

TABLE I
***d*-Spacings of Unmodified and Modified EVA–Clay Nanocomposites**

EVA–MAPP–clay (w/w)	*d*-Spacing (Å)
Cloisite 15A	33.4
98/0/2	36.2
95/0/5	36.8
88/10/2	36.8
85/10/5	38.0

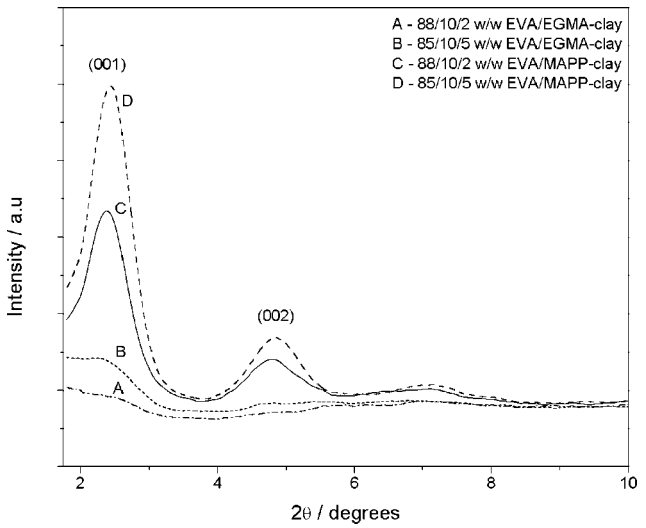

Figure 1 XRD patterns of (A) 88/10/2 EVA–MAPP–clay, (B) 85/10/5 EVA–MAPP–clay, (C) 88/10/2 EVA–EGMA–clay, and (D) 85/10/5 EVA–EGMA–clay.

EVA–clay nanocomposites, and the basal spacings are summarized in Table I. According to these spectra, there was some intercalation but there was no exfoliation. The (001) diffraction peak for the sample containing 5% clay was at $2\theta = 2.44^\circ$, corresponding to a basal spacing of 38 Å, whereas for the sample containing 2% clay, it was at $2\theta = 2.40^\circ$, corresponding to a basal spacing of 36.78 Å. Figure 2(A) shows a TEM micrograph of the sample containing 5% clay; there was very little intercalation, and there was no exfoliation (arrow A shows clay stacks, and arrow B may indicate exfoliation, but it probably indicates sample deformation as a result of sample cutting at room temperature). Figure 3(A) shows that for the 5% clay containing, EGMA-compatibilized nanocomposite, the clay platelets were distributed informally throughout the polymer matrix, and this should have improved the physical and permeability properties.

Figure 1(A,B) shows the XRD spectra of the EGMA-compatibilized EVA–clay nanocomposites. The almost complete disappearance of the (001) peaks of the clay indicates a highly exfoliated morphology, but the peak position ($2\theta = 2.4^\circ$) for the 5% clay containing sample indicates that there were some unintercalated clay

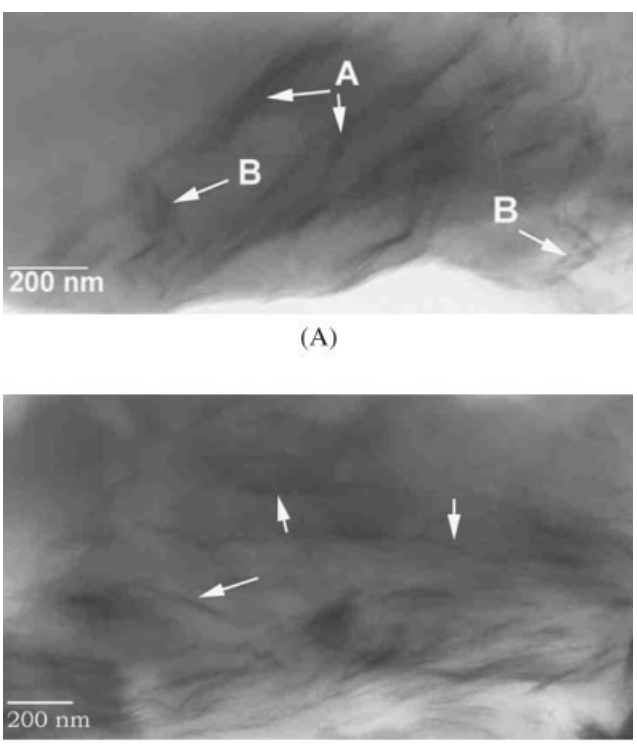

Figure 2 TEM images of (A) 85/10/5 EVA–MAPP–clay and (B) 85/10/5 EVA–EGMA–clay.

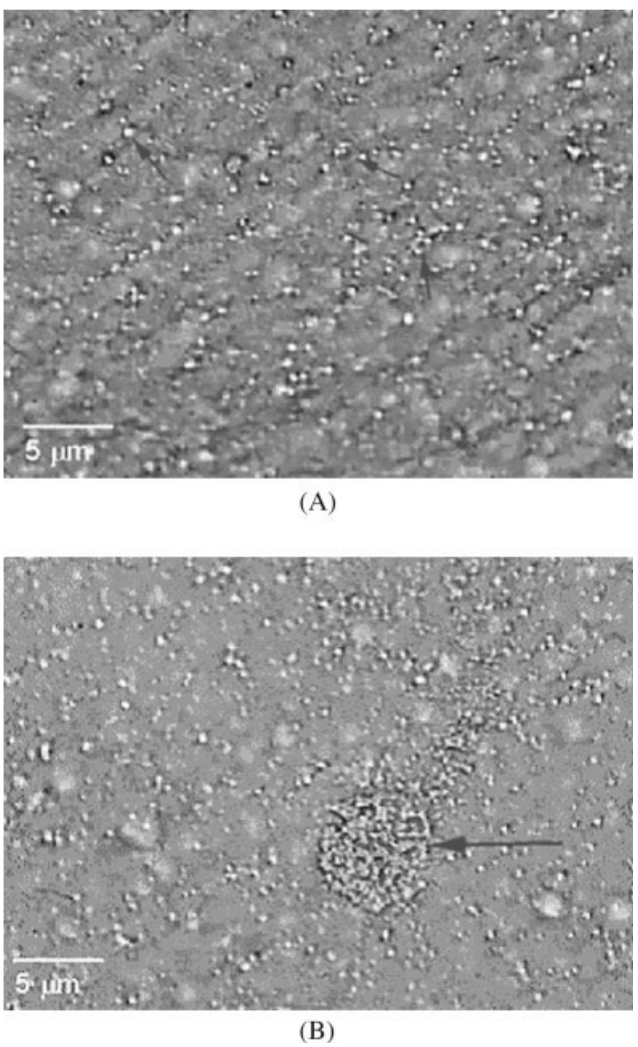

Figure 3 Scanning electron microscopy images of (A) 85/10/5 w/w EVA–EGMA–clay and (B) 85/10/5 w/w EVA–MAPP–clay.

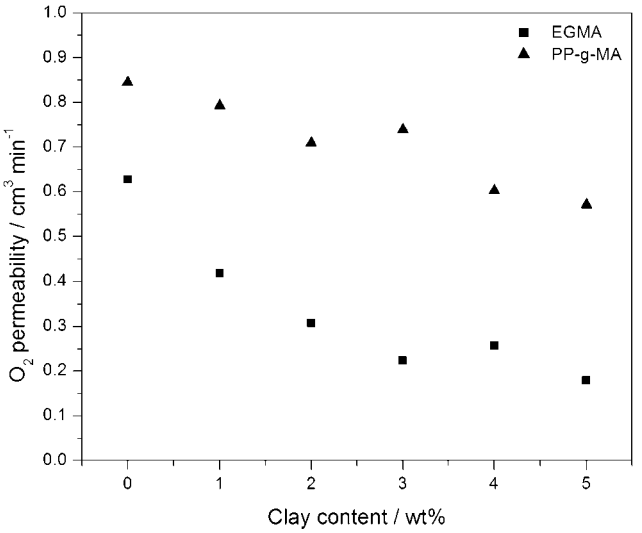

Figure 4 Oxygen permeability of compatibilized EVA–clay nanocomposites as a function of the clay content.

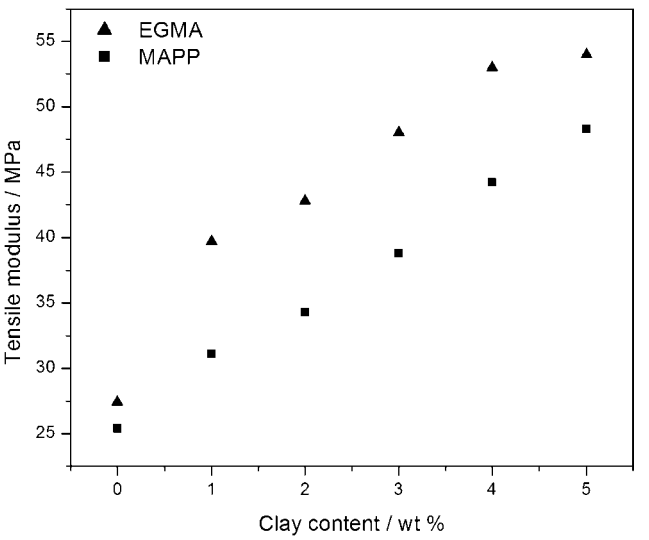

Figure 5 Tensile modulus of compatibilized EVA–clay nanocomposites as a function of the clay content.

stacks. The TEM image in Figure 2(B), which clearly shows well-developed exfoliation as well as some clay stacks, confirms this observation. Clay intercalation is also obvious in this figure. From the XRD spectra, it is clear that the 2% clay containing sample was more exfoliated than the 5% clay containing sample. Figure 3(B) clearly shows aggregation of the clay particles, with accompanying weaker interactions between the matrix and the clay particles and reduced physical and permeability properties.

Polymer–clay nanocomposites can also be used for packaging or storage tank applications in which the nanodispersed clay layers reduce the permeability of the polymer matrix. The presence of silicate layers in nanocomposites increases the diffusion distance by creating a tortuous path that the diffusing species must traverse.[25] Figure 3 shows the oxygen gas permeability as a function of the weight percentage of clay for samples with 10% compatibilizer. The gas permeability strongly depends on the morphology of the nanocomposites. Figure 4 shows that the O_2 permeability decreased with increasing clay content with EGMA and MAPP as compatibilizers. The presence of EGMA, however, reduced the permeability much more than the presence of MAPP, even in the absence of any clay. It could therefore be expected that EGMA-compatibilized nanocomposites would have much lower permeability than MAPP-compatibilized nanocomposites. Added to this is the much more exfoliated nature of the EGMA-compatibilized nanocomposites, which probably contributed to the reduction in the oxygen permeability. The permeability values are also presented in Table II.

TABLE II
Oxygen Permeability of Compatibilized EVA–Clay Nanocomposites

Sample	O_2 permeability (cm^3/min)	
	EGMA	MAPP
Pure EVA	0.615	0.615
Pure EGMA	0.620	—
Pure MAPP	—	1.016
89/10/1 (w/w) EVA–compatibilizer–clay	0.419	0.847
88/10/2 (w/w) EVA–compatibilizer–clay	0.308	0.709
87/10/3 (w/w) EVA–compatibilizer–clay	0.224	0.738
86/10/4 (w/w) EVA–compatibilizer–clay	0.258	0.602
85/10/5 (w/w) EVA–compatibilizer–clay	0.179	0.571

The average values for the tensile properties of the samples are presented in Figures 5–7 and in Table III. The tensile modulus (Fig. 5) increased signifi-

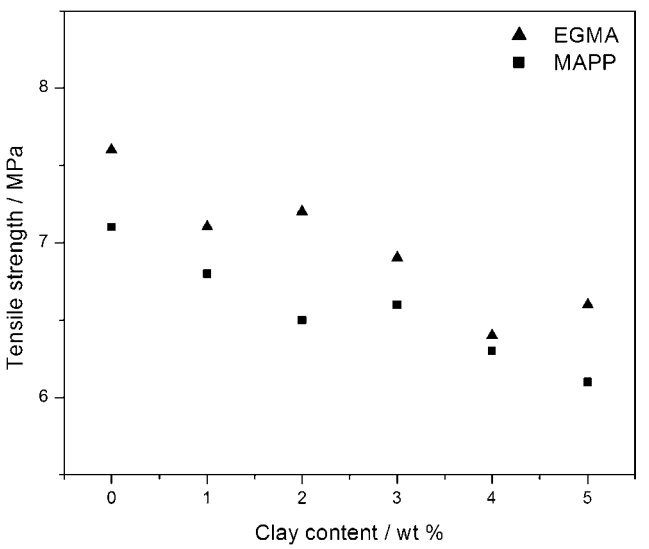

Figure 6 Tensile strength of compatibilized EVA–clay nanocomposites as a function of the clay content.

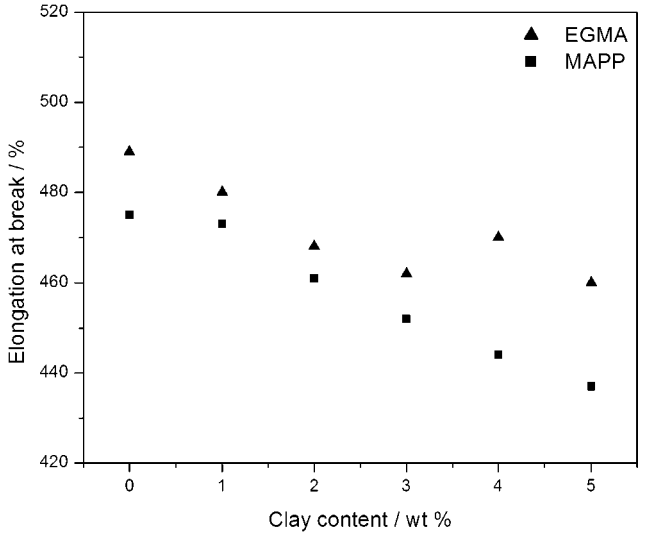

Figure 7 Elongation at break of compatibilized EVA–clay nanocomposites as a function of the clay content.

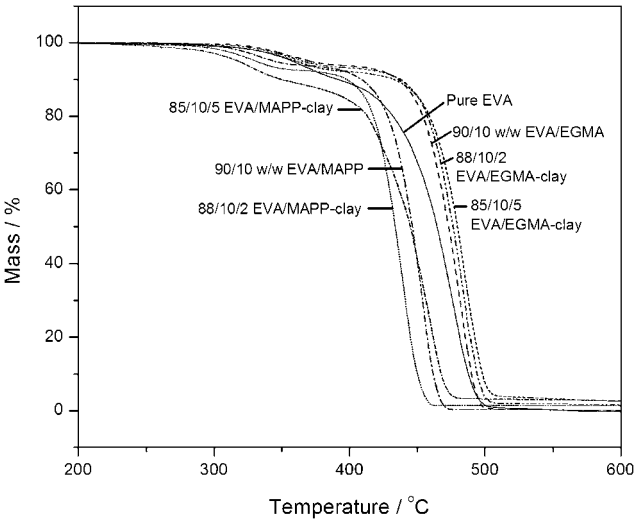

Figure 8 TGA curves of pure EVA, EVA–compatibilizer blends, and compatibilized EVA–clay nanocomposites.

cantly with increasing clay content for both systems. The tensile strength and elongation (Figs. 6 and 7), however, decreased slightly with increasing clay content in the nanocomposites. Generally, the tensile properties of the EGMA-compatibilized nanocomposites were better than those of the MAPP-compatibilized nanocomposites. There are two reasons for this observation. The 90/10 (w/w) EVA–EGMA blend showed higher values for all three these tensile properties than the 90/10 (w/w) EVA–MAPP blend. The difference in the tensile strength and elongation at break between the EGMA- and MAPP-compatibilized composites could therefore be primarily attributed to the presence of EGMA and MAPP, respectively, in the samples. Figure 5, however, shows differences between the tensile moduli of the EGMA- and MAPP-compatibilized composites and the EVA–EGMA and EVA–MAPP blends. It is thus clear that the modulus was influenced not only by the presence of the compatibilizer but also by the effect of the compatibilizer on the intercalation/exfoliation of the clay in the matrix. The XRD results show clear exfoliation in the case of the EGMA-compatibilized composites, whereas the MAPP-compatibilized composites primarily had clay intercalation. The better matrix–clay interaction in the case of the EGMA-compatibilized composites therefore gave rise to lower chain mobility and higher moduli.

The TGA curves of the samples are presented in Figure 8. It does not seem as if the presence of clay strongly influenced the thermal stability of the samples. The MAPP-containing samples generally showed lower thermal stability than pure EVA, whereas the EGMA-containing samples generally showed higher thermal stability than pure EVA and the MAPP-containing samples, probably because

TABLE III
Tensile Properties of Compatibilized EVA–Clay Nanocomposites

Sample	Tensile modulus (MPa)	Tensile strength (MPa)	Elongation at break (%)
Pure EVA	24.5 ± 2.6	7.8 ± 0.2	552 ± 15
90/10 (w/w) EVA–EGMA	27.4 ± 2.0	7.6 ± 0.2	489 ± 10
90/10 (w/w) EVA–MAPP	25.4 ± 2.1	7.1 ± 0.2	451 ± 7
89/10/1 (w/w) EVA–EGMA–clay	39.7 ± 1.0	6.6 ± 0.2	480 ± 13
88/10/2 (w/w) EVA–EGMA–clay	42.8 ± 2.8	7.2 ± 0.2	468 ± 8
87/10/3 (w/w) EVA–EGMA–clay	48.0 ± 2.5	6.9 ± 0.2	462 ± 5
86/10/4 (w/w) EVA–EGMA–clay	53.0 ± 3.7	6.4 ± 0.2	470 ± 13
85/10/5 (w/w) EVA–EGMA–clay	54.0 ± 2.3	6.6 ± 0.2	460 ± 11
89/10/1 (w/w) EVA–MAPP–clay	31.1 ± 2.0	6.8 ± 0.2	473 ± 14
88/10/2 (w/w) EVA–MAPP–clay	38.8 ± 2.5	6.5 ± 0.3	461 ± 12
87/10/3 (w/w) EVA–MAPP–clay	34.3 ± 1.9	6.6 ± 0.3	452 ± 5
86/10/4 (w/w) EVA–MAPP–clay	44.2 ± 2.7	6.3 ± 0.2	444 ± 10
85/10/5 (w/w) EVA–MAPP–clay	48.3 ± 1.5	6.1 ± 0.3	437 ± 13

EGMA itself is thermally more stable than EVA and MAPP. There was also little difference between the thermal degradation behaviors of the EVA–EGMA blend and the EVA–EGMA–clay composites. There were, however, obvious differences between the thermal degradation behavior of the EVA–MAPP blend and the EVA–MAPP–clay composites. The onset temperatures of the first and second degradation steps, as well as the decomposition rate of the second step, clearly decreased with increasing clay content. It seems as if the clay (or organic modifier) catalyzed the degradation of MAPP, which produced free radicals that initiated the early degradation of EVA.

CONCLUSIONS

The influence of EGMA and MAPP as compatibilizers on the physical properties of EVA–clay nanocomposites was investigated. The MAPP-compatibilized nanocomposites had intercalated and partially exfoliated structures, whereas the EGMA-compatibilized nanocomposites had completely exfoliated structures. The EGMA-compatibilized nanocomposites were thermally more stable than the MAPP-compatibilized nanocomposites. The mechanical and permeability properties of the EGMA-compatibilized nanocomposites were better than those of the MAPP-compatibilized nanocomposites.

Remy Bucher at Themba Labs in Somerset-West, South Africa, performed the X-ray diffraction analyses of the samples.

References

1. LeBaron, P. C.; Wang, Z.; Pinnavaia, T. J Appl Clay Sci 1999, 15, 11.
2. Okada, A.; Usuki, A. Mater Sci Eng C 1995, 3, 109.
3. Kato, M.; Usuki, A.; Okada, A. J Appl Polym Sci 1997, 66, 1781.
4. Kawasumi, M.; Hasegawa, N.; Kato, M.; Usuki, A.; Okada, A. Macromolecules 1997, 30, 6333.
5. Reichert, P.; Nitz, H.; Kinke, S.; Brandsch, R. I.; Thomann, R.; Mülhaupt, R. Macromol Mater Eng 2000, 275, 8.
6. Usuki, A.; Kato, M.; Okada, A.; Turauchi, T. J Appl Polym Sci 1997, 63, 137.
7. Vaia, R. A.; Giannelis, E. P. Macromolecules 1997, 30, 7990.
8. Hackett, E.; Manias, E.; Giannelis, E. P. J Chem Phys 1998, 108, 7410.
9. Zhang, Y. Q.; Lee, J. H.; Jang, H. J.; Nah, C. W. Compos B 2004, 35, 133.
10. Giannelis, E. P. Adv Mater 1996, 8, 29.
11. Oya, A.; Kurokawa, Y.; Yasuda, H. J Mater Sci 2000, 35, 1045.
12. Garcés, J. M.; Moll, D. J.; Bicerano, J.; Fibiger, R. C.; McLeod, D. G. Adv Mater 2000, 12, 1835.
13. Kojima, Y.; Usuki, A.; Kawasumi, M.; Okada, A.; Fukushima, Y.; Kurauchi, T. J Mater Res 1993, 8, 1185.
14. Lan, T.; Pinnavaia, T. J. Chem Mater 1994, 6, 2216.
15. Vaia, R. A.; Isii, H.; Giannelis, E. P. Chem Mater 1993, 5, 1694.
16. Wang, S.; Yuan, H.; Song, L.; Wang, Z.; Chen, Z.; Fan, W. Polym Degrad Stab 2002, 77, 423.
17. Giannelis, E. P.; Krishnamoorti, R. K.; Manias, E. Adv Polym Sci 1999, 138, 107.
18. Alexandre, M.; Beyer, G.; Herrist, C.; Cloots, R.; Rulmont, A.; Jerome, R.; Dubois, P. Macromol Rapid Commun 2001, 22, 643.
19. Zanetti, M.; Camino, G.; Thomann, R.; Mulhaupt, R. Polymer 2001, 42, 4501.
20. Zhang, J.; Wilkie, C. A. Polym Degrad Stab 2003, 80, 163.
21. Kato, M.; Okamoto, H.; Hasegawa, N.; Tsukigase, A.; Usuki, A. Polym Eng Sci 2003, 43, 1312.
22. Hotta, S.; Paul, D. R. Polymer 2004, 45, 7639.
23. Lee, J. H.; Jung, D.; Hong, C. E.; Rhee, K. Y.; Advani, S. G. Compos Sci Technol 2005, 65, 1996.
24. Guduri, B. R.; Luyt, A. S. J Appl Polym Sci 2007, 103, 4095.
25. Paulo, M.; Syed, Q. Thermochim Acta 2006, 442, 74.